Silver Nanoscale Antisense Drug Delivery System for Photoactivated Gene Silencing

ARTICLE *in* ACS NANO · MARCH 2013

Impact Factor: 12.88 · DOI: 10.1021/nn304868y · Source: PubMed

5 AUTHORS, INCLUDING:

Paige Brown Jarreau
Louisiana State University
13 PUBLICATIONS **412** CITATIONS
SEE PROFILE

Ammar Qureshi
Naval Medical Research Center
20 PUBLICATIONS **137** CITATIONS
SEE PROFILE

Daniel J Hayes
Louisiana State University
42 PUBLICATIONS **547** CITATIONS
SEE PROFILE

Silver Nanoscale Antisense Drug Delivery System for Photoactivated Gene Silencing

Paige K. Brown, Ammar T. Qureshi, Alyson N. Moll, Daniel J. Hayes,[†] and W. Todd Monroe*,[†]

Biological and Agricultural Engineering, Louisiana State University and LSU AgCenter, Baton Rouge, Louisiana 70803, United States. [†]These senior authors contributed equally to this work.

ABSTRACT The unique photophysical properties of noble metal nanoparticles contribute to their potential as photoactivated drug delivery vectors. Here we demonstrate the synthesis and characterization of 60−80 nm silver nanoparticles (SNPs) decorated with thiol-terminated photolabile DNA oligonucleotides. *In vitro* assays and fluorescent confocal microscopy of treated cell cultures show efficient UV-wavelength photoactivation of surface-tethered caged ISIS2302 antisense oligonucleotides possessing internal photocleavable linkers. As a demonstration of the advantages of these novel nanocarriers, we investigate properties including: enhanced stability to nucleases, increased hybridization activity upon photorelease, and efficient cellular uptake as compared to commercial transfection vectors. Their potential as multicomponent delivery agents for oligonucleotide therapeutics is shown through regulation of ICAM-1 (Intracellular Adhesion Molecule-1) silencing. Our results suggest a means to achieve light-triggered, spatiotemporally controlled gene silencing *via* nontoxic silver nanocarriers, which hold promise as tailorable platforms for nanomedicine, gene expression studies, and genetic therapies.

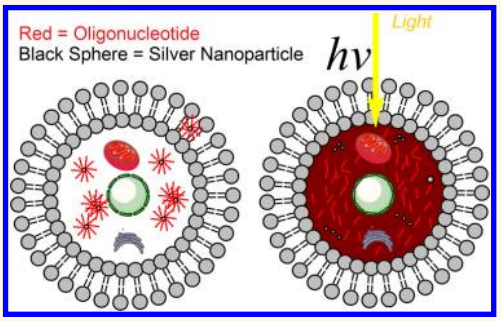

KEYWORDS: silver nanoparticles · drug delivery · photoactivation · antisense therapeutics · nanomedicine

Targeted delivery and controlled release of oligonucleotide therapeutics *in vivo* are essential aspects of an ideal delivery vehicle.[1] In this study we have undertaken the synthesis and *in vitro*/intracellular characterization of silver nanoparticle (SNP) photolabile nucleic acid conjugates, with the aim of developing a platform for inducible gene silencing. Due to unique size-related properties, nanostructures are increasingly utilized for intracellular diagnostics and delivery applications.[2] The majority of current nanoscale delivery platforms are polymeric in composition. However, studies of metallic nanoparticles have highlighted their suitability for delivery of various therapeutic agents including small molecules,[3,4] antisense oligonucleotides,[5,6] and siRNAs.[7,8] The potential benefits of noble metal nanoparticles in delivery applications include tunable size and shape, ease of bulk synthesis *via* "wet chemistry" techniques,[9] large surface-area-to-volume ratios, simple covalent functionalization chemistries,[9] and enhanced stability of surface-bound nucleic acids.[10,11] Nanoscale silver is one of the optically-active surface-enhancing substrates available.[12,13] SNP-based single delivery platforms incorporate solutions to both intracellular detection and external control over surface-tethered drug release *via* chemical,[14] photothermal,[10,15] or photochemical[16] triggers.

Here we report the synthesis of UV-photoactivated SNP nanocarriers of antisense therapeutics which, when compared to free nucleic acids, exhibit enhanced stability, increased resistance to enzymatic degradation, enhanced cellular uptake, and controllable restoration of therapeutic activity upon photoactivation. Silver has not traditionally been applied in nanoparticle-based drug delivery applications, where gold[5−7] and other materials[17] have been popular, likely due to difficulty of SNP synthesis and functionalization, reduced stability when functionalized according to popular salt-aging techniques, and concerns about silver toxicity. However, clinical use of SNPs as effective antimicrobial solutions in wound care, as well as recent *in vivo* studies providing positive safety assessments for systemic

* Address correspondence to tmonroe@lsu.edu.

Received for review February 3, 2012 and accepted March 8, 2013.

Published online March 08, 2013
10.1021/nn304868y

exposure, have encouraged biomedical research with SNPs.[18−21] A 2008 animal study revealed minimal induction of secondary markers of liver damage even in the presence of chronic oral SNP doses greater than 300 mg/kg/day for 28 days.[22] Reported safety and lack of side effects for SNPs administered at "moderate" doses[23] may lend greater confidence to the suitability of SNPs for *in vivo* biomedical solutions especially considering studies that seek to lower the threshold of "effective" SNP doses by harnessing their large drug payload capabilities and electromagnetic field amplifying characteristics. Recent improvements in SNP biocompatibility *via* surface modification, as well as exceptional optical properties,[13,24] have also improved suitability of SNPs for drug delivery. The unique field enhancement properties of SNPs, where the light scattering cross section of a silver nanoparticle is ~10 times greater than that of a similarly sized gold nanoparticle,[13] have led to increased interest in their use as sensors,[25,26] biological labels,[13] and substrates for surface-enhanced absorption, fluorescence,[27] and photochemistry.[12,28] Additionally, SNPs offer higher extinction coefficients and blue-shifted plasmon resonant peaks over other metallic nanomaterials,[13,24] making them an appropriate alternative for photocontrolled drug delivery applications and potential surface-enhanced photochemistry of caged compounds such as nitrobenzyl derivatives. Our SNP platform (Figure 1a) for antisense drug delivery and spatiotemporal release takes advantage of silver's unique photophysical properties for fluorescence confirmation of surface functionalization, cell uptake, and activation *via* nitrophenylethyl (NPE) nucleic acid linker photocleavage.

RESULTS AND DISCUSSION

A new platform for enhanced delivery of antisense therapeutics and photoactivated gene silencing with *in situ* detection of activation could augment gene expression analysis, clinical antisense therapies and the study of genetic diseases. Our designed SNP-oligonucleotide conjugates display desirable properties as gene delivery agents: enhanced cellular uptake, increased oligonucleotide stability or therapeutic lifetime, and a steric caged effect of the nanocarrier with light-inducible activation.

SNP Synthesis. A citrate reduction SNP synthesis method was chosen due to ease of bulk synthesis within the desired size range (60−80 nm in diameter) for maximal field enhancement properties,[29] optimal size for cellular uptake,[30] and simple *in situ* exchange of the sodium citrate capping moieties. Synthesized colloids were characterized *via* UV−vis spectroscopy to reveal a broad absorbance spectrum centered around 420 nm (Figure 1b), characteristic of citrate-reduced SNPs in this size-range, with a shoulder around 345 nm attributable to multipole resonance modes,[13] and absorbance above 550 nm due to aggregates or larger rod-like structures.[31] Transmission electron microscopy (TEM) images show an average

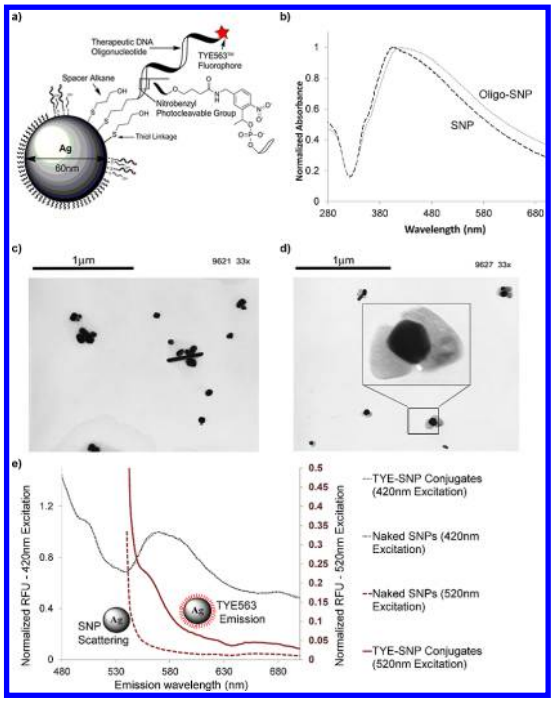

Figure 1. Concept and characterization of SNPs and SNP-oligo conjugates. (a) Schematic of caged oligonucleotide-functionalized SNPs (oligo-SNPs). (b) Normalized absorbance spectra for SNPs and oligo-SNPs. (c) TEM images of SNP and (d) oligo-SNPs. (e) Fluorimetry scans of SNPs *vs* oligo-SNPs with TYE563 fluorophore conjugates, excited at 420 nm and 520 nm. Black lines represent 420 nm excited spectra (represented on the left axis); red lines represent 520 nm excited spectra (represented on the right axis). Spectra were normalized on the maximum signal obtained from 420 nm excitation. Inset pictures demonstrate SNP *vs* oligo-SNPs.

nonfunctionalized particle diameter of 68 nm ±18 nm (s.d.; Figure 1c). Inductively coupled plasma optical emission spectroscopy (ICP-OES) yielded a SNP concentration of 66.16 ± 2.6 ppm, and a theoretical yield of 84 pM based on the approximate mean spherical particle diameter from TEM.[13,24]

Functionalized SNP Characterization. SNP-oligo conjugates were synthesized *via* ligand exchange of citrate with 3′ thiol-modified DNA oligonucleotides and mercaptopropanol as an alkane spacer during a Tris salt aging process adapted from methods for gold nanoparticles.[32] A 48 h salt aging in amine-containing buffer reduced nonspecific oligo-particle interactions, critical in developing stable photosensitive SNP-conjugates. SNP-tethered oligonucleotides (SNP-TYE-NPE(1n)-oligo) were synthesized with a distal TYE563 fluorophore and an internal nitrobenzyl photocleavable linker (NPE) located at a distance of one nucleotide (1n) from the proximal alkane thiol modification. When exposed to UV light, the NPE linker initiates disengagement of a functional 20-mer antisense oligonucleotide from the protected nanoparticle surface (schematic (a) in Figure 1). An incorporated 10-mer thymine linker enhanced ligand packing on the SNP surface. Physiochemical characteristics of SNP-oligo conjugates, including

oligonucleotide coverage, stability, and surface properties, were analyzed *via* UV−visible spectroscopy, TEM, and fluorescence-based analysis techniques.

UV−visible spectroscopy serves to probe changes in the local dielectric environment and resulting changes in surface plasmon resonance (SPR) spectra that occur upon absorption of ligands[12,33] as described by Mie Theory.[34] Salt aging ligand functionalization of the SNP surface results in damping of SPR peak intensity and red-shifting of the resonance peak.[33] These phenomena were observed in our synthesized SNP-oligo conjugates, with slight red-shifting evidence of ligand attachment (Figure 1b). SNP-conjugates remained stable during subsequent treatments including centrifugation, resuspension, UV-light exposure, and cellular delivery.

TEM analysis of citrate stabilized and oligonucleotide functionalized SNPs (Figure 1c,d) reveal an average citrate stabilized SNP diameter of 68 ± 18 nm (s.d.), and an average SNP-oligo conjugate diameter of 74 ± 21 nm (s.d.), based on image analysis ($n = 50$, $P > 0.05$). The average SNP-Thiol-oligo conjugate diameter was confirmed *via* dynamic light scattering (DLS) (*Z* average diameter = 75.95 nm, PdI = 0.241). SNP morphologies were varied with a predominance of spherical or spheroidal particles, characteristic of citrate ion reduction methods.[35] SNP-thiol oligo conjugates in Figure 1d and inset show surrounding regions of reduced density, possibly from adsorbed oligonucleotides and associated salts. TEM sample preparation and imaging may have affected these tethered oligonucleotide layers.

Spectra of citrate stabilized SNPs and purified SNP-TYE-NPE(1n)-oligo conjugates (Figure 1e) reveal broad scattering signals when excited at 420 nm. An excitation line at 420 nm was chosen for proximity to the SNP SPR absorbance peak. While there is a curve shown for citrate stabilized SNP illuminated at 420 nm, it is not different than the signal from TYE-SNP (as the TYE fluorophore is not efficiently excited at 420 nm). Emission spectra (excitation 520 nm) indicate TYE563-labeled oligonucleotide attachment to SNP surfaces in functionalized samples. The signal from these samples under constant illumination at 420 nm or 520 nm is likely scattering from the SNP and fluorescence of the TYE fluorophore (as shown distinctly different in citrate stabilized and TYE-SNP samples).

DNA Coverage Quantification. Oligonucleotide coverage on the nanoparticle surface is important in determining conjugate stability, efficiency of therapeutic delivery, and availability of attached oligonucleotides for hybridization.[36] Loading density is impacted by salt concentration, oligonucleotide sequence, monolayer composition, and particle properties, including size and radius of curvature.[37,38] A fluorescence-based method for quantifying surface coverage, similar to that used by Demers *et al.*,[39] yields an SNP-TYE-NPE(1n)-oligo coverage density of 7.56(±2) × 10^{12} oligonucleotides/cm^2, with a ligand footprint[38] of 13.2 ± 2 nm^2. These values, calculated for 68 nm diameter SNPs and a surface coverage ratio of 855:1 oligonucleotides per particle, are comparable to those reported previously for DNA-functionalized gold nanoparticles of similar dimensions (reported coverage and footprint for 60 nm gold particles 7.8(±1)10^{12} oligos/cm^2 and 13 ± 2 nm^2, respectively) using PBS-buffer based salt aging processes.[38] Complete oligonucleotide removal with DTT resulted in particle aggregation and red-shifting of SPR spectra, typical of ligand desorption.[39]

***In Vitro* Hybridization Activity.** *In vitro* hybridization studies indicate a steric-caged phenomenon for SNP-tethered oligonucleotides. Attachment to the SNP surface prevents oligo-target hybridization until photorelease is initiated. A molecular beacon (MB) was used to compare hybridization activity between SNP-oligo conjugates and oligonucleotides displaced from SNPs with DTT. Increases in FITC beacon fluorescence, with concomitant quenching of TYE563-labeled oligonucleotide fluorescence, indicates an increase in hybridization following chemical release of oligonucleotides from the SNP surface (Figure 2-Ia). Following chemical release of ligand, solution fluorescence measurements were taken in the absence of nanoparticles to reduce signal interference. These solution measurements were confirmed by gel electrophoresis (Figure 2-Ib), and similar results were obtained following light triggered release. In this case, the SNP serves as a bulky caging group, inactivating the attached nucleic acid until photoactivation restores hybridization.

***In Vitro* Protection from Nuclease Degradation.** SNP-tethered TYE563-labeled oligonucleotides were effectively protected from DNase I nuclease action (Figure 2-IIa, *top*), confirming a previously observed phenomenon with gold nanoparticles.[11] Similarly treated free-solution TYE563-labeled oligonucleotide samples suffered significant nuclease degradation over the course of 15 min (Figure 2-IIb, *top*). TYE fluorescence measurements of aspirated solution following centrifugation of DNase I treated SNP-oligo conjugates also confirmed minimal nuclease degradation from nanoparticle surfaces (*data not shown*). Digestion of these and other similarly tethered oligonucleotide complexes with serum and specific intracellular nucleases (*e.g.*, DNase II)[40] is a worthwhile follow-on endeavor, particularly considering that their endo/lysosomal trafficking has not been thoroughly studied.

***In Vitro* Photorelease and Photorelease Efficiency.** The release of oligonucleotides with internal NPE linkers from the surface of SNPs was achieved at irradiation wavelengths of 302 nm and 365 nm. UV−vis spectra were monitored throughout functionalization, UV-light exposure, and chemical (DTT) mediated release of oligonucleotides (Figure 3a). Slight red-shifting in the photoexposed sample may be attributed to slight particle aggregation, mediated by joule heating or reduced Debye shielding. Exaggerated SPR red-shifting in DTT-treated samples was observed as expected and attributed to

aggregation following ligand desorption. Minimal aggregation in photoexposed samples is important in the design of the construct, as the 1-mer nucleotide groups remaining on the surface help prevent aggregation, similar to the stabilizing effects of polyelectrolytes on small SNPs previously reported.[41] The NPE group also remains on the SNP following photocleavage, preventing free intracellular nitrosoketone photoproducts seen with many nitrobenzyl-caged compounds, which have been shown to damage cellular systems.[36] Fluorescence data for photoreleased TYE563-labeled oligonucleotide ligands demonstrate effective purification (*sample 2*) and photocleavage (*sample 3*) of oligonucleotides from SNP-oligo conjugates (Figure 3b).

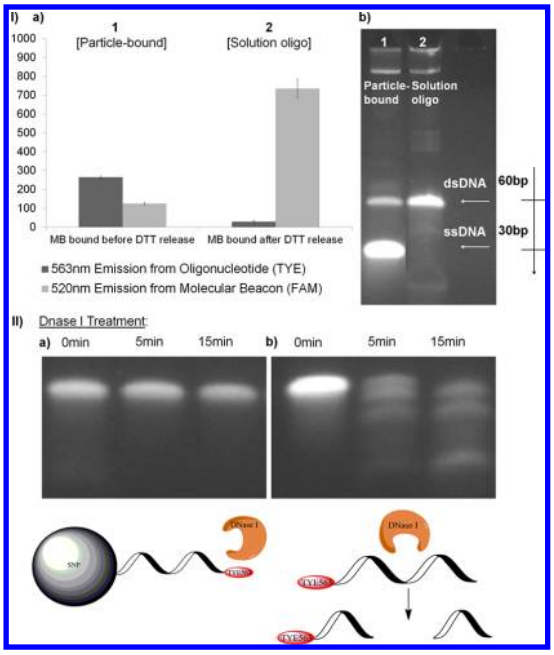

Figure 2. Activity of particle-bound *vs* released oligonucleotide ligands. (I) Hybridization data. (a) Graph of solution fluorescence data for FAM-labeled molecular beacon (MB) and TYE563-labeled thiol-modified oligonucleotide. Sample 1, hybridization of a complementary MB to particle-bound oligonucleotide; sample 2, hybridization of a complementary MB to particle-released oligonucleotide, as measured by open-beacon FAM fluorescence and TYE quenching by the beacon's BHQ1. Error bars represent standard deviation of duplicate samples. (b) Gel electrophoresis run of samples 1 and 2. (II) DNase I digestion assay of particle-bound *vs* solution-phase oligonucleotides. (*top*) Gel electrophoresis runs of (b) nuclease digested solution-phase samples and (a) post-treatment-DTT-removed particle-bound samples at 0, 5, and 15 min nuclease treatment times. (*bottom*) Schematic of DNase I activity on (b) solution-phase and (a) particle-bound oligonucleotide.

The maximum yields of photoconversion at both low (302 nm) and high (365 nm) wavelength ranges reached 50−60% of total ligand, based upon comparison of photoreleased TYE563-labeled oligonucleotide fluorescence intensity with chemically released ligand. Light dose response plots reveal an expected progression of photoconversion with increasing dose for nitrophenylethyl-containing oligonucleotides (Figure 3c). Calculated functional quantum yields (ϕ_{fn})[42] of SNP-tethered NPE linkers, with a particle-to-NPE-linker distance of 2−3 nm, were $\phi_{fn320nm} = 0.16$ and 0.04 at irradiation wavelengths of 320 and 365 nm, respectively. These values are comparable to reported functional quantum yields of caged nucleic acids.[43] Extinction coefficients were calculated based on absorbance spectroscopy of internal NPE linkers ($\varepsilon_{320nm} = 3520\ M^{-1}\ cm^{-2}$; $\varepsilon_{365nm} = 3520\ M^{-1}\ cm^{-2}$). This functional quantum (ϕ_{fn}) yield was chosen for evaluating SNP-oligonucleotide activation as a measure of total ligand release and not merely NPE cleavage as seen with traditional quantum yields of small caged molecules. It is important to distinguish that a single NPE group is sufficient to transiently tether and thus block bioactivity of the oligonucleotide in this design, which is deemed to be superior to traditional caged oligonucleotide approaches, where several photocage moieties are necessary to block hybridization and thus require greater doses of light for photoactivation.[42] Preliminary studies of particle-to-NPE-linker distances indicate higher quantum yields at distances of 2−3 nm,

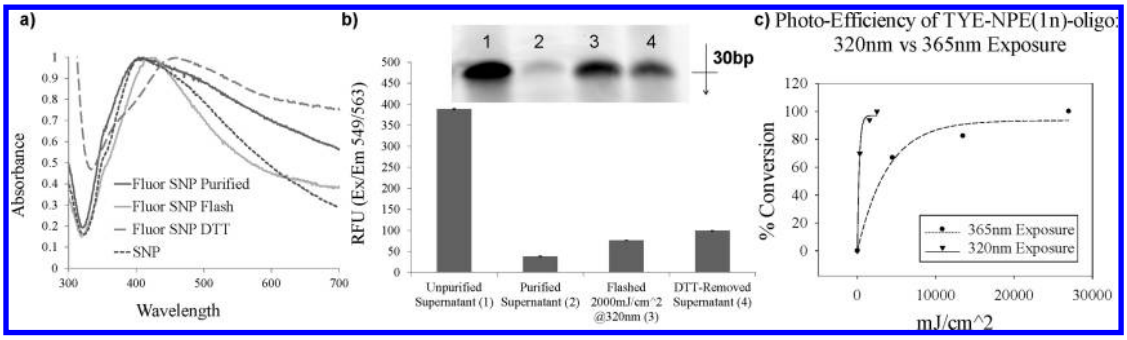

Figure 3. Photorelease from SNP surfaces. (a) Normalized absorbance spectra for nonfunctionalized silver nanoparticles (SNP), purified photosensitive SNP-oligo conjugates (Fluor SNP Purified), light-irradiated SNP-oligo conjugates (Fluor SNP Flash), and SNPs following DTT-mediated removal of surface oligonucleotides (Fluor SNP DTT). (b) Graph fluorescence intensity for TYE-labeled oligonucleotide removed from nanoparticle surfaces *via* (1 and 2) centrifugation, (3) flashing, and (4) DTT treatment. Error bars represent standard deviation of fluorimeter readings for each sample. Inset: Gel electrophoresis run of samples 1−4. (c) Photorelease profiles of TYE-NPE(1n)-oligo from SNP-oligo conjugate surface at 320 nm (5.2 mW/cm^2) and 365 nm (206 mW/cm^2), in units of percent conversion to released state from SNP-tethered state of photolabile oligonucleotides. Curves represent exponential rise-to-max trendlines for experimental data.

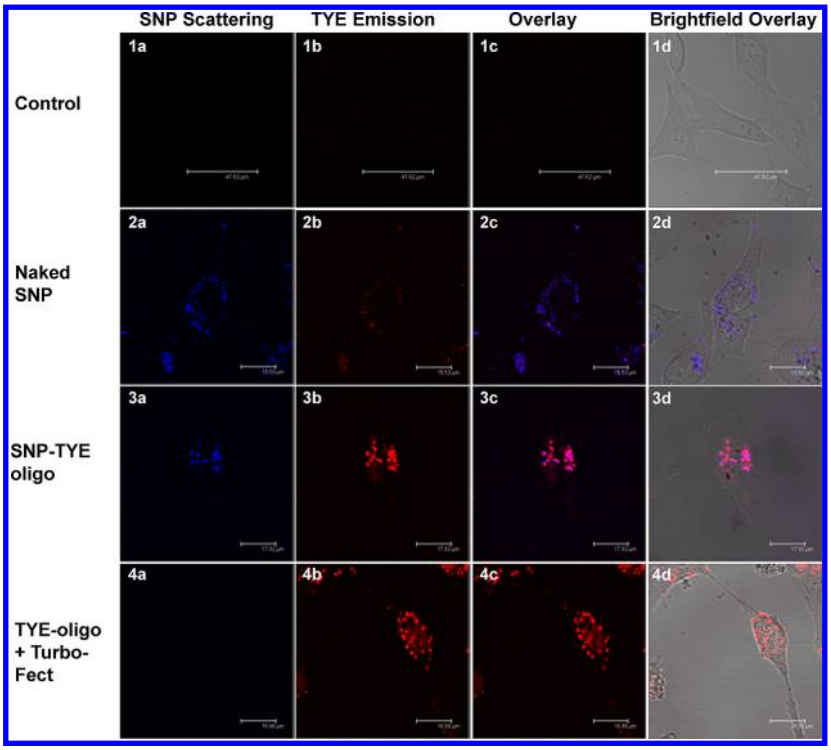

Figure 4. SNP-TYE-NPE(1n)-oligo delivery to HeLa cells. (1) Control *vs* (2) SNP treated *vs* (3) SNP-TYE-NPE(1n)-oligo conjugate treated *vs* (4) phosphodiester TYE-oligo treated HeLa cells. Images depict (a) silver particle scattering (488/520 nm), (b) TYE fluorescence (549/563 nm), (c) fluorescence overlay, and (d) brightfield views. SNPs exhibit a wide range of scattering, explaining appearance of faint silver signal in the TYE563 channel (see image *2b*).

compared to 5−6 nm from the silver surface (Supporting Information, Supplementary Figure 7, Supplementary Table 1). Future distance-dependent studies are necessary for optimization of surface photochemistry and photorelease.

Confocal Microscopy Analysis of SNP-Conjugate Delivery and Photorelease Profile. Fluorescence confocal imaging of HeLa cell cultures confirmed SNP-oligo conjugate intracellular delivery, ligand photorelease, subcellular localization, and photoactivated antisense activity. Confocal images indicate intracellular delivery of SNP-oligonucleotide conjugates and photorelease of oligonucleotides in situ. Delivery of SNP-oligo conjugates to the intracellular environment was achieved without the use of chemical transfection vectors traditionally required (Figure 4, image series 3 *vs* series 4). Reflectance mode images of SNPs were acquired by epi-illumination, permitting facile detection of SNP within cells. Localization of SNP-oligo conjugates in the intracellular space was assessed *via* 3-dimensional reconstruction of thin-slice image stacks (Supporting Information, Supplementary Figures 4 and 5). Flow cytometric analysis was also used to confirm SNP-oligo conjugate uptake in HeLa cells, where large increases in fluorescence are observed in cells containing the conjugates (Supporting Information, Supplementary Figure 11). Gating on the fluorescence of the TYE665 fluorophore used in the SNP-oligo conjugates for these studies, an average of 98.44% of cells treated with a 1× dose indicated positive uptake. Staining SNP-treated cells with LysoTracker probes of both dark and photoexposed samples did not show complete colocalization of these signals that would be indicative of sole lysosomal entrapment (Supporting Information, Supplementary Figure 8). Overlay of particle scattering at 488 nm with TYE-labeled oligonucleotide fluorescence indicates colocalization of oligonucleotides with SNPs in the absence of UV-light exposure (Figure 4 image *3c*). Citrate stabilized SNPs were also transported to the cytosol, suggesting transmembrane internalization based primarily on the particle properties (size, morphology, charge; Figure 4, images *2a*, *2c*). Citrate stabilized and functionalized SNPs were found to reside primarily in the cytosolic environment, the ideal localization in mRNA-targeting antisense applications.

Intracellular redistribution of labeled oligonucleotides upon photoexposure of SNP-oligo conjugates was also demonstrated *via* confocal microscopy (Figure 5). In all nonexposed samples, TYE-labeled oligonucleotide fluorescence colocalized with SNP scattering (Figure 5, image series *1*), in a punctuate pattern within the cell (schematic I in Figure 5). Colocalization of TYE563 and silver scattering indicates that conjugates are stable and remain intact after 16−24 h within the intracellular environment. However, upon UV-irradiation of cells treated with photolabile SNP-oligo conjugates, a diffusion of oligonucleotide fluorescence (Figure 5, images *2b*, *3b*)

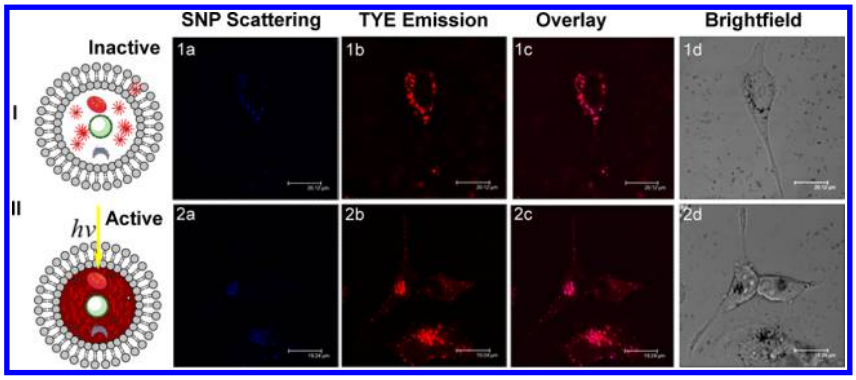

Figure 5. Photoreleased SNP-TYE-NPE(1n)-oligo. I. Schematic of intracellular (a) particle-bound oligonucleotide ligand *vs* (b) photoreleased ligand. II. (1) Nonreleased *vs* (2) photoreleased SNP-TYE-NPE(1n)-oligo conjugates samples. Images depict (a) particle scattering (488/488 nm), (b) TYE fluorescence (549/563 nm), (c) overlay, and (d) brightfield views. Particle signals are false-colored in blue for ease of visualization of overlay regions in red.

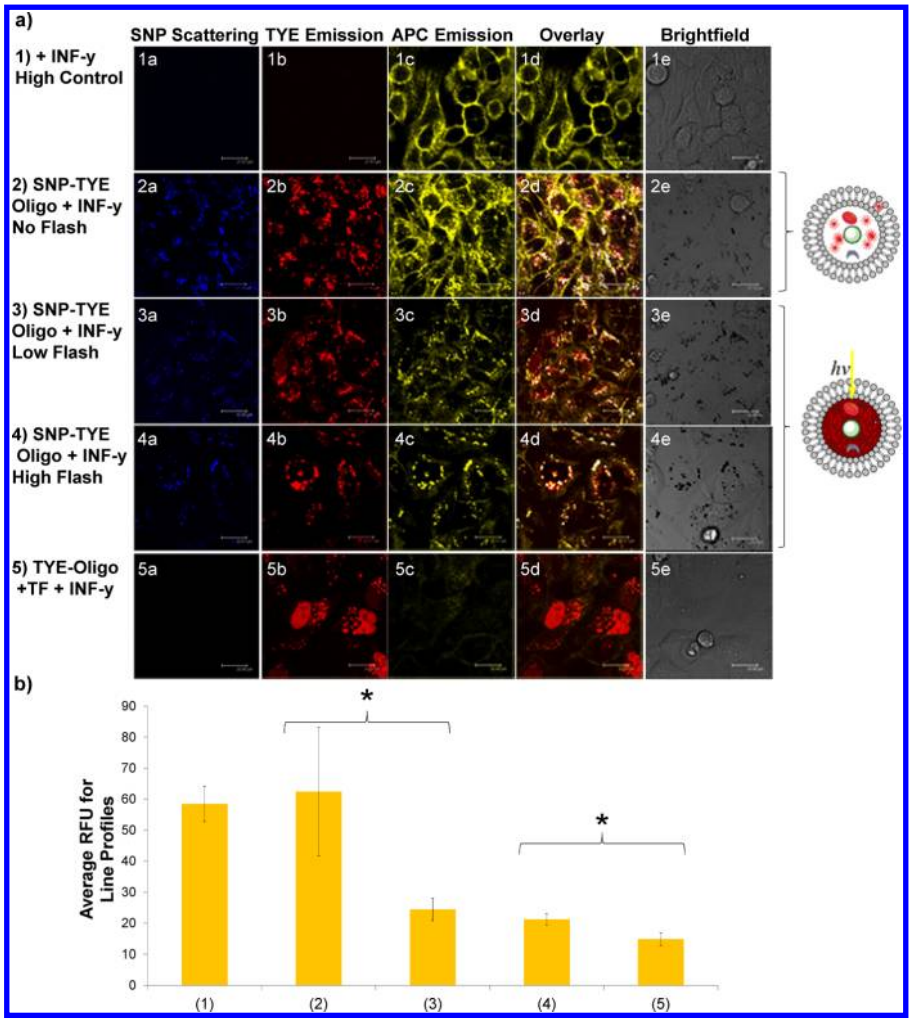

Figure 6. Antisense activity of photoactivated SNP-TYE-NPE(1n)-oligo conjugates. (a) CD54-expressing HeLa cells (1) without antisense treatment are compared to SNP-oligo conjugate treated cells in both (2) nonactivated and (3, 4) photoactivated cases. (5) TurboFect (TF) transfected TYE-oligo treated HeLa cells are used as a control case. Images depict (a) silver particle scattering (488/488 nm), (b) TYE fluorescence (549/563 nm), (c) APC-conjugated antihuman CD54 fluorescence (633/680), (d) overlay, and (e) brightfield views. SNPs exhibit a wide range of scattering, explaining appearance of faint silver signal in the TYE563 channel (see image *2b*). Overlay regions are magenta (SNP scattering plus TYE emission) and white (SNP, TYE, plus APC emission). (b) Cell periphery fluorescence line scans of cells in representative images for APC-antibody labeling intensities. Errors are standard deviation of the mean, and significance was determined using Student's *t* test (*$P < 0.01$; $n > 3$). P value for sample 2 *vs* sample 3: 0.0002; *P* value for sample 4 *vs* sample 5: 0.006.

reflects release of functional oligonucleotides from particle surfaces and increased availability of these for binding to mRNA targets within the cytosol. These data agree with other reports of metallic NP assisted, light-induced payload release within the cytosol of living cells.[44−47] Unique in this application is, to our knowledge, the first demonstration of phototriggered chemical dissociation of nucleic acids in the intracellular space. Sequestration of oligonucleotides within the nucleus, often observed for cells treated *via* commercially available lipid or polymer transfection agents, was not observed for the SNP-oligo conjugates.

Antisense Activity of SNP-Oligo Conjugates. Confocal microscopy results demonstrate the successful delivery and photocaged effect of SNP carriers for antisense DNA oligonucleotides. SNP-bound ISIS2302 antisense oligonucleotides, which target ICAM-1(CD54) mRNA, decreased the expression level of CD54 upon photoactivation (Figure 6). Successful knockdown, evidenced by reduced membrane labeling of antihuman CD54 antibody, is apparent when comparing nonexposed (Figure 6a, images *2c,d*) and exposed (Figure 6a, images *3c, d, 4c,d*) SNP-oligo treated cells. Similar to results from Figure 5, photoreleased TYE-oligo can be seen as diffuse cytosolic fluorescence, noting that it can be differentiated from cell periphery antibody staining (Figure 6a, images *3d, 4d*). It is important to note that the appearance of broadly scattering nanoparticles in the APC-labeled antibody emission images can be differentiated from membrane antibody staining due to differences in localization. Citrate-stabilized SNPs at similar concentrations have no effect on CD54 expression in both UV-exposed and nonexposed conditions (*data not shown*). Free solution phosphodiester TYE-oligo was used as an antisense control, loaded at higher concentrations *via* TurboFect polymer transfection agent and showing strong knockdown activity (Figure 6a, images *5a−e*). Comparing the location of these polymer-complexed TYE-oligonucleotides *versus* SNP-oligo conjugates revealed less nuclear entrapment of SNP-oligos, suggesting greater potential for mRNA interactions in the intended cytosolic compartment *via* APC-antibody labeling was quantified *via* fluorescence line scans (Leica Software) on cell peripheries, similar to methods reported elsewhere.[48] Average antibody fluorescence over periphery line scans indicate significant increase in SNP-oligo antisense activity upon photoactivation (Figure 6b, graph). There was no significant difference between average antibody staining intensities in control and nonexposed SNP-oligo cases, indicating no leak in antisense activity in the noninduced state. Additionally, there was no effect of these 365 nm light doses on HeLa viability, morphology or CD54 expression (Supporting Information, Supplementary Figure 6; UVA photoeffects on HeLa cells from this source also detailed inref 49). Similarly, there were no effects of SNPs on HeLa cell viability (Supporting Information, Supplementary Figure 8), and only minimal decreases in cell viability were observed at 10- and 50-fold doses above those used in the antisense activity experiments.

CONCLUSIONS

We have demonstrated the facile synthesis and functionalization of ∼60 nm (average diameter) silver nanoparticles with thiol-capped nitrophenylethyl (NPE) linker-containing oligonucleotides, and their intracellular characterization as photoactivated nanocarriers of antisense therapeutics. Previous reports of photoresponsive metal nanoparticles note evidence that a nanoscale metal core may deactivate excited states of photoactive units near a plasmon resonant surface.[50] However, the photochemistry of the internal NPE linker in this system was fully functional 2−3 nm from SNP surfaces. The enhancement factor of absorption, fluorescence, or photoconversion at or near a silver surface will depend on particle shape and size, as well as the distance of the photoactive molecule from the particle surface.[51] SNPs with ∼50 nm diameters have shown the greatest intensity of local fields and surface enhanced fluorescence.[29] There are additional methods of metallic NP synthesis and functionalization at high concentration, which could provide better morphological control and higher colloidal stability.[19,52−54] Many of these methods of synthesis could be utilized to then form oligo-NP conjugates for use in photoactivation, as demonstrated herein. Future studies are planned to explore the modulation of photocleavage by tuned localized surface plasmon resonance (LSPR) in these *versus* NPs of other composition (*e.g.*, gold[44,46,47]).

Quenching of photochemical processes can occur in molecules directly adsorbed or tethered to within 1 nm of the metal surface, where the energy transfer from the excited molecule to the metal surface competes with the accumulation of energy by the molecule.[55] Thus, an important consideration in these studies was the tethered distance of the NPE linker, to strike a compromise between photochemistry enhancement and nonradiative damping[56] or quenching processes. A separation of ∼2−3 nm was appropriate for release of SNP-tethered oligonucleotide therapeutics using UV-light exposure doses unharmful to cell cultures. No more light was required for photorelease of oligonucleotides from SNPs than for photocleavage of the same oligonucleotides in solution. Distance-dependent photoreactivity of SNP-tethered linkers could be further elucidated through investigation of various particle-to-NPE-linker distances to determine optimal conjugate design for photoactivation. Optimal distances for surface-enhanced photochemistry will depend on compound reaction rates and nonradiative decay rates to the metal surface,[28] orientation of photoactive compounds to the surface,[57] and particle size and morphology.[58] However, favorable distances

will theoretically reside within a range proportionate to the substrate particle radius due to significant decay of near-field enhancements beyond this range.

The broad range of SNP optical properties was utilized for confirmation of SNP-antisense conjugate delivery and intracellular drug release. This platform provided nuclease resistance of tethered antisense oligonucleotides and enhanced their cellular uptake and intracellular diffusion upon photorelease. Importantly, delivery of SNP-oligos was accomplished without the need for additional transfection vectors. Efficiency of SNP-mediated delivery of antisense oligonucleotides to the intracellular environment was comparable to a commercial polyethylenimine-based transfection agent, considering factors including amount, rate, and distribution of oligonucleotide delivery, as well as post-transfection cell health. These results corroborate previous studies demonstrating enhanced delivery of gold oligonucleotide conjugates based on dense surface charge, associated salt, and adsorbed proteins in serum media;[6] with SNPs adding photoactivation and more pronounced particle tracking capabilities.

The light-induced cytosolic redistribution of SNP delivered oligonucleotides indicates augmented availability of oligonucleotide for hybridization to mRNA targets. This was confirmed by the antisense activity of photoactivated SNP-ISIS2302-oligonucleotide conjugates against Intracellular Adhesion Molecule-1 (ICAM-1). ICAM-1 is targeted in inflammation disorders such as Crohn's disease, and antisense treatment of its overexpression has been conducted clinically using the ISIS2302 sequence.[59] Our assays demonstrated, in addition to successful delivery and release, a caged phenomenon for antisense oligonucleotides attached to SNP surfaces in the absence of external phototriggers, which can restore their therapeutic activity. With the advancement of new controlled targeting and release agents, a prized goal in nanomedicine,[60] an SNP caging system permitting photocontrolled, spatiotemporal gene silencing holds promise as an alternative or supplement to existing drug delivery platforms. To date, caged oligonucleotides have been used in the laboratory to control gene expression in zebrafish for developmental studies,[61−64] precisely apply gradients of gene silencing,[65] or better understand and create synthetic genetic circuits,[66] but could one day be uniquely suited for optically accessible clinical applications in dentistry, opthamology, dermatology, and pulmonary cases (reviewed in ref 36). While the small penetration depth of photoactivating UVA wavelengths will not likely permit deep tissue targeting without direct fiber delivery approaches (as demonstrated in ref 67), doses can be optimized to achieve photoactivation *in vitro*[49] and *in vivo*[68] without significant biological damage. The SNP caging platform demonstrated here could be adapted for use in many of the aforementioned laboratory and clinical applications, and is a step toward light-sensitive intelligent delivery systems[69] with improved pharmacokinetic properties and precisely controlled activity *in vivo*.

With future studies, we hope to further characterize the effect of SNP field-enhancement on linker photochemistry with the aim to increase ϕ_{fn} and increase photoactivation wavelengths. Additional future work includes investigating SNP-conjugate systems with increased protection and photoactivated antisense activity against a variety of gene targets *in vivo*.

METHODS

SNP Synthesis Functionalization. Silver nitrate (SigmaUltra >99%) and sodium citrate were purchased from Sigma Aldrich (St. Louis, MO). Other materials for SNP synthesis included PTFE coated stir-bars (VWR, West Chester, PA), 100 mL glass syringes (KD scientific, Holliston, MA), and SNP synthesis-reserved glassware (Fisher Scientific, Pittsburgh, PA). Silver surfaces were functionalized with custom thiol-modified oligonucleotides ordered from Integrated DNA Technologies (IDT, Coralville, IA). A 2 M Tris-NaCl buffer (pH 8.0) was made up from Biotechnology grade Tris (Amresco Inc., Solon, OH) and sodium chloride (Fischer Scientific, Pittsburgh, PA). Dithiothreitol (1 M aqueous) purchased from Sigma (St. Louis, MO) was employed for DTT-mediated oligonucleotide removal from SNP surfaces.

SNP Synthesis. Citrate-reduced silver colloid was prepared according to a modified Lee and Meisel method.[70] Silver nitrate (90 mg) was suspended in distilled water (500 mL) and heated rapidly to boiling (95−100 °C) under continuous stirring. Upon boiling, a 1.0% solution of sodium citrate (10 mL) was added dropwise with a syringe-pump automated flow rate (0.5 mL/min), while solution color progression from pale yellow to dark green signified formation of silver colloid. The solution was allowed to boil for the duration of citrate addition, plus 10 min following addition, to ensure complete reduction of silver nitrate. The colloid was allowed to cool to room temperature prior to characterization *via* visible absorption spectroscopy and transmission electron microscopy (TEM). Once synthesized, the colloid was stable for 2−3 weeks at 4 °C.

Design of SNP-Conjugate Oligonucleotides. The photolabile oligonucleotides for conjugation to SNP surfaces were designed in such a manner as to optimize surface coverage, SNP-conjugate stability, and surface-enhancement of photochemical processes, including fluorescence detection and photolysis of the nitrophenylethyl (NPE) internal photocleavable linker. A 10mer thymine linker was incorporated into the 3′ thiol-modified oligonucleotides in order to enhance particle surface coverage due to the fact that thymine has been previously shown to have the least affinity for metal surfaces of the four available nucleotides,[71] thus, reducing nonspecific oligo-metal interactions. Spacer thiols have also been shown to reduce the nonspecific adsorption of nucleic acids onto metal particle surfaces[36] by competing for surface attachment sites, thus, an alkane spacer thiol (mercaptopropanol) has been incorporated which adsorbs to the metal surface concurrently with the target oligonucleotide.

The particle-bound oligonucleotides (Supporting Information, Supplementary Figure 1) have as their base the ISIS2302 sequence, which is an established antisense sequence against ICAM-1 (CD54).[59] This system served as a proof of concept in

studies on SNP-mediated antisense drug delivery and controlled release. A simple thiol-modified ISIS2302 sequence oligonucleotide (Supporting Information, **1a** in Supplementary Figure 1) was used as a control for immobilization of nucleic acid onto silver surfaces and characterization of surface coverage. A TYE(563) fluorophore-labeled oligonucleotide was designed for fluorescence detection of oligonucleotide in solution and attached to SNPs. The excitation/emission (549/563 nm) properties and particle-fluor spacing (10−12 nm based on a 30mer separating oligonucleotide sequence) were chosen to minimize overlap with intrinsic SNP fluorescent properties in the SPR region and quenching by the silver surface. Of the two oligonucleotides studied for photocleavage analysis, the photocleavable group in the TYE-NPE(1n)-oligo (Supporting Information, **2a** in Supplementary Figure 1) is spaced from the particle surface by a three carbon alkane thiol linker plus one thymine nucleotide, while the photocleavable group in the NPE(10n)-oligo (Supporting Information, **2b** in Supplementary Figure 1) is spaced from the particle by the three carbon alkane thiol plus a thymine linker sequence of 10 nucleotides. The thiol linker is estimated to have a linear length <1 nm, based on reported C−C, C−S, and S−Ag bond lengths,[72] and the nitrobenzyl linker an estimated linear length slightly greater than 1 nm based on traditional bond lengths. Oligonucleotide length is estimated based on a 0.3−0.35 nm/base unit length.[73] This leads to particle-to-photolabile linker distances for the SNP-TYE-NPE(1n)-oligo conjugates and SNP-NPE(10n)-oligo conjugates of 2−3 and 5−6 nm, respectively. The different particle to photocleavable group spacing distances will serve to help evaluate distance-dependent influences of silver surface plasmon resonance on the NPE photochemical reaction.

SNP Functionalization. Silver nanoparticles were functionalized *via* a modified "salt-aging" technique. Custom thiol-modified TYE563-labeled oligonucleotides (Integrated DNA Technologies, Inc.) were mixed with silver colloid at a oligo-to-particle stoichiometry of 5000:1 and left to incubate at 37 °C under gentle rocking conditions to favor initial oligonucleotide. Following a 24 h incubation period, a 48 h Tris-buffer based salt-aging process was commenced during which the SNP-oligo conjugate solution was first rapidly adjusted to 1% SDS and 25 mM phosphate buffer, and subsequently slowly (4× 10 μL aliquot additions of a 1 M Tris-NaCl buffer per 24 h) adjusted to 80 mM NaCl and 80 mM Tris buffer (pH 8.0) concentration. Functionalized nanoparticles were purified *via* centrifugation (3 × 7000 rpm) and resuspended in a modified buffer (1% SDS, 50 mM Tris-NaCl) prior to experimental analysis.

Citrate Stabilized and Functionalized SNP Characterization. For UV−visible and fluorescence spectroscopic characterization, citrate and oligonucleotide functionalized SNPs were diluted to appropriate concentrations in DI water. Diluted samples were analyzed for absorption properties in a wavelength range scan (200−700 nm), and for single excitation (420 nm and 520 nm), multiple emission fluorescence properties using a PE LSB-50 spectrofluorimeter. Spectra were normalized to maximum SPR absorption and particle scattering or fluorescence signals.

For TEM characterization, 5 μL of SNP solution and 5 μL of SNP-Thiol-oligo conjugate (with no NPE photolabile linker) solution were pipetted on carbon/copper 20−30 nm grids (EMS, Hatfield, PA), air-dried, and visualized with JEOL 100CX. MetaVue image analysis (Universal Imaging Corporation, West Chester, PA) was employed to determine particle counts and average particle size from TEM images.

DNA Coverage Quantification. DNA coverage on functionalized SNP-TYE-NPE(1n)-oligo conjugates was quantified *via* fluorescence-based measurements and confirmed *via* gel electrophoresis of particle-released oligonucleotide samples. Following SNP-conjugate functionalization and purification *via* centrifugation (3 × 7000 rpm), 1% dithiothreitol (DTT) was added to SNP-oligo solutions and allowed to shake at 37 °C for 10−15 min. Following an additional purification step to remove DTT-released oligonucleotide from silver colloid (1 × 7000 rpm), released oligonucleotide-supernatant was analyzed *via* fluorimetry with excitation/emission lines set at 549/563 nm (TYE fluorescence spectra, Integrated DNA Technologies, Coralville, IA) on a PE LSB-50 spectrofluorimeter. A TYE-oligo fluorescence calibration curve was used to indirectly quantify TYE-oligo coverage on SNP surfaces based on solution measurements (Supporting Information, Supplementary Figure 3). The SNPs were quantified using inductively coupled plasma optical emission spectroscopy (ICP-OES). The SNP pellet was resuspended in 1 mL DI water, incubated with 1 mL nitric acid, transferred to weighed ICP vials, agitated for 2.5 h, and diluted to a final volume of 10 mL with acidified water. The final vials were weighed and the diluted samples analyzed with Varian Vista MPX (Palo Alto, CA).

***In Vitro* Hybridization Activity.** Hybridization activity studies were carried out following SNP functionalization and conjugate purification. A FAM-BHQ molecular beacon with a sequence complementary to the ISIS2302 sequence of the oligonucleotide ligands was hybridized to both SNP-bound and SNP-released oligonucleotide samples (see hybridization assay schematic in Supporting Information, Supplementary Figure 2). Hybridization conditions were 30 min at 60 °C followed by 15 min at 4 °C. These conditions were chosen based on a T_M of 40.7 °C for the highest energy hairpin folding structure of the molecular beacon (IDT SciTools mFold, Coralville, IA). Releasing conditions included both UV-light exposure and 1% DTT treatment. Oligonucleotide and oligonucleotide-beacon duplex samples were purified and removed from silver nanoparticle surfaces prior to fluorescence analysis *via* fluorimetry with excitation/emission lines set at 549/563 nm for TYE-fluorescence and 480/520 nm for FAM-fluorescence. For SNP-bound samples, FAM-BHQ molecular beacon was added to 500 μL of SNP-oligo conjugates at a final concentration of 0.6 μM (0.3 nmoles). Following hybridization, free molecular beacon was removed *via* centrifugation (1 × 7000 rpm), and oligonucleotide and duplex ligands were removed from particle surfaces *via* DTT treatment (1 × 7000 rpm) for fluorescence and gel analysis. For SNP-released samples, oligonucleotide was removed *via* DTT after which FAM-BHQ molecular beacon was added, hybridized, and purified from SNP surfaces (1 × 7000 rpm) similar to above. Fluorescence and gel analysis provided comparison of ssDNA *vs* DNA-beacon duplex in both SNP-bound and SNP-released cases. A solution hybridization control was run *via* gel electrophoresis (0.15 nmoles FAM-BHQ molecular beacon, 0.05 nmoles TYE-oligo) to confirm gel results of experimental samples. All samples were desalted *via* spin columns (3 kDa Amicon Ultra filters, Millipore, Billerica, MA) and dried *via* vacuum centrifuge to a final volume of <10 μL for final gel preparation. Samples were analyzed *via* UV-gel electrophoresis and Sybr Green staining (Invitrogen Corporation, Carlsbad, CA).

***In Vitro* Protection from Nuclease Activity.** Protection of SNP-bound oligonucleotides from nuclease activity was investigated *via* a DNase I digestion assay on free solution DNA and surface-bound DNA alike. 1 mL of prepared SNP-TYE-NPE(1n)-oligo conjugate was purified *via* centrifugation (2 × 7000 rpm) and resuspended in 500 mL of 1× DNase I NEB buffer (New England BioLabs, Ipswich, MA). Free solution TYE-labeled oligonucleotide (1.5 μg) was also suspended in 500 mL of 1× DNase I NEB buffer prior to DNase I digestion. 4U of DNase I (stock concentration 2U/ml) was added to sample solutions and incubated at 37 °C for intervals of 5 and 15 min. Following digestion intervals, DNase stop buffer (0.5 M EDTA) was added to each sample to a final concentration of 5 mM. SNP-TYE-NPE(1n)-oligo conjugates were purified *via* centrifugation (1 × 7000 rpm) followed by 1% DTT-mediated removal of DNA as described previously. Free solution and particle-bound DNA samples were desalted *via* spin columns (3 kDa Amicon Ultra filters, Millipore, Billerica, MA) and dried *via* vacuum centrifuge to a final volume of <10 μL. Samples were analyzed *via* gel electrophoresis and fluorescent-gel imaging (Typhoon 8600, GE Healthcare Life Sciences, Piscataway, NJ).

***In Vitro* Photorelease Efficiency.** Proof of photolabile oligonucleotide release from particle surfaces was demonstrated *via* solution fluorescence and fluorescent gel electrophoresis mediated detection of TYE-labeled nucleic acid ligands. A total of 1 mL of prepared SNP-TYE-NPE(1n)-oligo conjugates were loaded in a demountable quartz cuvette chamber (5 mm path length, 49-Q-5, Starna Cells Inc., Atascadero, CA) and irradiated at 320 nm with a UVP-Transilluminator with a fluence of 5.2 mW/cm^2 or at 365 nm with a GreenSpot system (American Ultraviolet, Lebanon, IN), which incorporates a 100 watt, pressurized mercury lamp with 5 × 1000 mm^2 light guide, and produces a peak spectral

output at 365 nm (American Ultraviolet, Lebanon, IN). The lamp has a fluence of 206 mW/cm^2 with the short bandpass (1.5 mm thick, 2.4 mm diameter SWP-2502U-400, Lambda Research Optics, CA) and IR filters (818-ST-UV detector, Newport Corporation, Irvine, CA) in place.[49] Released oligonucleotides were purified *via* centrifugation (1 × 7000 rpm) from SNP substrates in order to conduct fluorimetry and fluorescent gel electrophoresis (Typhoon 8600, Excitation laser: 532 nm, Emission filter: 560LP) analysis. Extinction coefficient values for the internal NPE linker were calculated according to absorption values found by absorption spectroscopy of TYE-NPE(1n)-oligonucleotide with an incorporated NPE photocleavable linker.

Cell Culture. HeLa cells (human epithelial carcinoma cells, American Type Culture Collection) were maintained in 25 cm^2 flasks (BD Falcon, Franklin Lakes, NJ) with 5 mL of Dulbecco's modified Eagle's medium-reduced serum (DMEM-RS, Hyclone Thermo Scientific, Logan, UT) supplemented with 3% fetal bovine serum (FBS, Hyclone Thermo Scientific, Logan, UT) and incubated at 37 °C in a humidified atmosphere containing 5% CO_2. Opti-MEM (OM, Invitrogen Corporation, Carlsbad, CA) is a reduced protein nonphenol-red medium which was used for imaging purposes.

Confocal Microscopy Analysis of SNP-Conjugate Delivery, Subcellular Localization, Photorelease Profile. Confocal microscopy was used to monitor SNP-oligo conjugate intracellular delivery, trafficking, and photorelease. For imaging purposes, HeLa cells were seeded in 1.0 borosilicate coverglass Lab-Tek 8-well chambered slides (Thermo Fisher Scientific, Rochester, NY). Final cell media volume in each chamber well was 400 μL. Cells were allowed to incubate for 24 h in DMEM+FBS media at 37 °C prior to SNP-oligo conjugate treatment. 5 μL of 1× naked SNPs and 5 μL of concentrated 5× SNP-oligo conjugates (≈1−2 μg oligo) were added directly to culture eight wells. Treated cells were incubated at 37 °C in a CO_2 incubator for 16 h following addition prior to live confocal imaging. For subcellular localization of SNPs *vs* lysosomes, treated cells were stained with LysoTracker (Invitrogen Corporation, Carlsbad, CA) for 1 h at 50 nm staining concentration. For photorelease profile studies, cells were flashed for 3 min at 365 nm (18 J/cm^2) 2 h prior to imaging (16 h post SNP-TYE-NPE(1n)-oligo conjugate delivery). All samples were resuspended in Opti-MEM prior to imaging. The Leica TCS SP2 spectral confocal and multiphoton system used consists of a Leica DM IRE2 inverted microscope with a galvo-Z stage, equipped with Ar/Kr, He/Ne green, and He/Ne red lasers. Of the provided laser lines, excitation lasers at 488, 543, and 633 nm were used in imaging experiments, concurrently with tuned emission wavelength windows. Reflectance mode images of SNPs were acquired by epi-illumination, centering the emission wavelength directly on the 488 nm excitation line, collecting 483−493 nm wavelengths. This method produced a pronounced signal that coincided with the dark areas seen using brightfield microscopy. Images were analyzed using Leica Confocal Software (LCS) Lite (Leica Microsystems Heidelberg GmbH).

Antisense Activity of SNP-Oligo Conjugates. Antisense activity of SNP-oligo conjugates against plasma membrane surface protein ICAM1 in HeLa cells was monitored *via* confocal microscopy. HeLa cells were seeded as described above. ICAM1 antisense oligonucleotide transfection, in the presence of serum, was carried out 16 h prior to experimental analysis, *via* TurboFect cationic polymer for control phosphodiester TYE-labeled oligonucleotide delivery, and *via* the SNP platform for photoactivated oligonucleotide delivery. TurboFect-oligonucleotide polyplex samples were prepared by mixing 1.5 μg of TYE-NPE(1n)-oligonucleotide or a phosphorothioate ISIS2302 oligonucleotide with 0.8 μL of TurboFect stock reagent in 100 μL OM for 15 min at room temperature and then added directly to DMEM+FBS in culture 8-wells in a 1:5 volumetric ratio. SNP-TYE-NPE(1n)-oligo conjugates were added to culture wells as described previously. ICAM1 was upregulated in HeLa cell samples with recombinant human interferon-γ (INF-γ, 16.9 KDa, eBioscience, San Diego CA) by adding 10 μg/mL to culture wells 12 h prior to antihuman CD54-APC (Allophycocyanin) conjugated antibody staining (Mouse monoclonal to ICAM1, AbCam, Cambridge, MA) and confocal imaging. Photorelease of antisense ISIS2302 from SNP-TYE-NPE(1n)-oligo conjugate surfaces was effected by flashing at 365 nm 6 h post-INF-γ treatment and 6 h preimaging. Flashing doses were as follows: 15 J/cm^2 (low flash) and 25 J/cm^2 (high flash). Cells were rinsed with and stained in Opti-MEM with 2%BSA for 1 h with 10 μL CD54-APC antibody stock and finally resuspended in Opti-MEM for imaging. Confocal images (512 × 512 pixels, 8 bit gray scale) were taken with a 40× oil-immersion objective, with exciting laser lines set at 488/543/633 nm simultaneously. Anti-CD54-APC fluorescence (excitation/emission 633 nm/690 nm,) was acquired with detector gains set at a constant 700 V to minimize autofluorescence and SNP scattering interference. Image statistics of cell circumference line scans were collected using quantification tools in Leica Confocal Software (LCS) Lite. Statistics collected for circumference line scans represent mean ± s.d. of APC fluorescence intensity along the entire length of a poly line ROI. Student's *t* test (two-sample assuming unequal sample sizes, unequal variances) was employed to determine ICAM1 expression changes, with *P* (one-tail) ≤ 0.01 considered to be significant. At least three cells ($n > 3$) in each representative image for treatment cases (untreated, SNP-oligo treated, SNP-oligo treated with photoexposures, and antisense control oligo-treated) were subjected to circumference line scan quantification.

Conflict of Interest: The authors declare no competing financial interests.

Acknowledgment. We would like to thank Dr. Matt Brown of the LSU Socolofsky Microscopy Center and Marilyn Dietrich of the LSU Cytometry Facility for expert technical assistance. Funding was provided by the National Science Foundation (CBET-0748195 and CMMI-0963482) and the State of Louisiana Board of Regents Support Fund. This material is based upon work supported under an LSU Economic Development Assistantship and Donald Clayton Graduate Fellowship to P.K.B.

Supporting Information Available: Visual schematic of oligonucleotide design (Supplementary Figure 1), a visual schematic of the hybridization assay experimental design (Supplementary Figure 2), TYE-oligo calibration curve data (Supplementary Figure 3), and confocal 3D reconstruction images confirming particle location inside cytosolic environment of imaged cells (Supplementary Figures 4 and 5). Data from a light-dosing assay showing lack of UV-induced effects on HeLa viabililty and ICAM-1 expression (Supplementary Figure 6), photocleavage efficiency properties of SNP-bound photolabile oligonucleotide (Supplementary Figure 7, Supplementary Table 1), cytotoxicity assay methods and results showing no effects of these doses of SNP on HeLa cells (Supplementary Figure 9), and additional examples of diffuse cytosolic oligonucleotide fluorescence following photoactivation (Supplementary Figure 10), as well as flow cytometric analysis of SNP uptake in HeLa cells (Supplementary Figure 11). This material is available free of charge *via* the Internet at http://pubs.acs.org.

REFERENCES AND NOTES

1. Roth, C. M. Molecular and Cellular Barriers Limiting the Effectiveness of Antisense Oligonucleotides. *Biophys. J.* **2005**, *89*, 2286–2295.
2. Kumar, C. *Tissue, Cell and Organ Engineering*; Wiley-VCH Verlag GmbH & Co. KGaA: Weinheim, 2006; Vol. 9.
3. Agasti, S. S.; Chompoosor, A.; You, C. C.; Ghosh, P.; Kim, C. K.; Rotello, V. M. Photoregulated Release of Caged Anticancer Drugs from Gold Nanoparticles. *J. Am. Chem. Soc.* **2009**, *131*, 5728–5729.
4. Nakanishi, J.; Nakayama, H.; Shimizu, T.; Ishida, H.; Kikuchi, Y.; Yamaguchi, K.; Horiike, Y. Light-Regulated Activation of Cellular Signaling by Gold Nanoparticles That Capture and Release Amines. *J. Am. Chem. Soc.* **2009**, *131*, 3822–3823.
5. Rosi, N. L.; Giljohann, D. A.; Thaxton, C. S.; Lytton-Jean, A. K. R.; Han, M. S.; Mirkin, C. A. Oligonucleotide-Modified Gold Nanoparticles for Intracellular Gene Regulation. *Science* **2006**, *312*, 1027–1030.
6. Giljohann, D. A.; Seferos, D. S.; Patel, P. C.; Millstone, J. E.; Rosi, N. L.; Mirkin, C. A. Oligonucleotide Loading Determines Cellular Uptake of DNA-Modified Gold Nanoparticles. *Nano Lett.* **2007**, *7*, 3818–3821.

7. Giljohann, D. A.; Seferos, D. S.; Prigodich, A. E.; Patel, P. C.; Mirkin, C. A. Gene Regulation with Polyvalent siRNA-Nanoparticle Conjugates. *J. Am. Chem. Soc.* **2009**, *131*, 2072–2073.
8. Song, W. J.; Du, J. Z.; Sun, T. M.; Zhang, P. Z.; Wang, J. Gold Nanoparticles Capped with Polyethyleneimine for Enhanced siRNA Delivery. *Small* **2010**, *6*, 239–246.
9. Katz, E.; Willner, I. Integrated Nanoparticle-Biomolecule Hybrid Systems: Synthesis, Properties, and Applications. *Angew. Chem., Int. Ed.* **2004**, *43*, 6042–6108.
10. Ghosh, P.; Han, G.; De, M.; Kim, C. K.; Rotello, V. M. Gold Nanoparticles in Delivery Applications. *Adv. Drug Delivery Rev.* **2008**, *60*, 1307–1315.
11. Seferos, D. S.; Prigodich, A. E.; Giljohann, D. A.; Patel, P. C.; Mirkin, C. A. Polyvalent DNA Nanoparticle Conjugates Stabilize Nucleic Acids. *Nano Lett.* **2009**, *9*, 308–311.
12. Kamat, P. V. Photophysical, Photochemical and Photocatalytic Aspects of Metal Nanoparticles. *J. Phys. Chem. B* **2002**, *106*, 7729–7744.
13. Yguerabide, J.; Yguerabide, E. E. Light-Scattering Submicroscopic Particles As Highly Fluorescent Analogs and Their Use As Tracer Labels in Clinical and Biological Applications - I. Theory. *Anal. Biochem.* **1998**, *262*, 137–156.
14. Hong, R.; Han, G.; Fernandez, J. M.; Kim, B. J.; Forbes, N. S.; Rotello, V. M. Glutathione-Mediated Delivery and Release Using Monolayer Protected Nanoparticle Carriers. *J. Am. Chem. Soc.* **2006**, *128*, 1078–1079.
15. Angelatos, A. S.; Radt, B.; Caruso, F. Light-Responsive Polyelectrolyte/Gold Nanoparticle Microcapsules. *J. Phys. Chem. B* **2005**, *109*, 3071–3076.
16. Han, G.; You, C. C.; Kim, B. J.; Turingan, R. S.; Forbes, N. S.; Martin, C. T.; Rotello, V. M. Light-Regulated Release of DNA and Its Delivery to Nuclei by Means of Photolabile Gold Nanoparticles. *Angew. Chem., Int. Ed.* **2006**, *45*, 3165–3169.
17. Sokolova, V.; Epple, M. Inorganic Nanoparticles As Carriers of Nucleic Acids into Cells. *Angew. Chem., Int. Ed.* **2008**, *47*, 1382–1395.
18. Qureshi, A. T.; Terrell, L.; Monroe, W. T.; Dasa, V.; Janes, M. E.; Gimble, J. M.; Hayes, D. J. Antimicrobial Biocompatible Bioscaffolds for Orthopaedic Implants. *J. Tissue Eng. Regener. Med.* **2012**, DOI: 10.1002/term.1532.
19. Qureshi, A. T.; Monroe, W. T.; Lopez, M. J.; Janes, M. E.; Dasa, V.; Park, S.; Amirsadeghi, A.; Hayes, D. J. Biocompatible/Bioabsorbable Silver Nanocomposite Coatings. *J. Appl. Polym. Sci.* **2011**, *120*, 3042–3053.
20. Percival, S. L.; Bowler, P.; Woods, E. J. Assessing the Effect of an Antimicrobial Wound Dressing on Biofilms. *Wound Repair Regen.* **2008**, *16*, 52–57.
21. Rai, M.; Yadav, A.; Gade, A. Silver Nanoparticles As a New Generation of Antimicrobials. *Biotechnol. Adv.* **2009**, *27*, 76–83.
22. Kim, Y. S.; Kim, J. S.; Cho, H. S.; Rha, D. S.; Kim, J. M.; Park, J. D.; Choi, B. S.; Lim, R.; Chang, H. K.; Chung, Y. H.; et al. Twenty-Eight-Day Oral Toxicity, Genotoxicity, and Gender-Related Tissue Distribution of Silver Nanoparticles in Sprague-Dawley Rats. *Inhalation Toxicol.* **2008**, *20*, 575–583.
23. Tiwari, D. K.; Jin, T.; Behari, J. Dose-Dependent *In Vivo* Toxicity Assessment of Silver Nanoparticle in Wistar Rats. *Toxicol. Mech. Methods* **2011**, *21*, 13–24.
24. Yguerabide, J.; Yguerabide, E. E. Light-Scattering Submicroscopic Particles As Highly Fluorescent Analogs and Their Use As Tracer Labels in Clinical and Biological Applications: II. Experimental Characterization. *Anal. Biochem.* **1998**, *262*, 157–176.
25. Thompson, D. G.; Enright, A.; Faulds, K.; Smith, W. E.; Graham, D. Ultrasensitive DNA Detection Using Oligonucleotide-Silver Nanoparticle Conjugates. *Anal. Chem.* **2008**, *80*, 2805–2810.
26. Graham, D.; Faulds, K.; Thompson, D.; McKenzie, F.; Stokes, R.; Dalton, C.; Stevenson, R.; Alexander, J.; Garside, P.; McFarlane, E. Functionalized Nanoparticles for Bioanalysis by SERRS. *Biochem. Soc. Trans.* **2009**, *37*, 697–701.
27. Fu, Y.; Zhang, J.; Lakowicz, J. R. Plasmonic Enhancement of Single-Molecule Fluorescence near a Silver Nanoparticle. *J. Fluoresc.* **2007**, *17*, 811–816.
28. Wolkow, R. A.; Moskovits, M. Enhanced Photochemistry on Silver Surfaces. *J. Chem. Phys.* **1987**, *87*, 5858–5869.
29. Zhang, J.; Fu, Y.; Chowdhury, M. H.; Lakowicz, J. R. Single-Molecule Studies on Fluorescently Labeled Silver Particles: Effects of Particle Size. *J. Phys. Chem. C* **2008**, *112*, 18–26.
30. Chithrani, B. D.; Ghazani, A. A.; Chan, W. C. W. Determining the Size and Shape Dependence of Gold Nanoparticle Uptake into Mammalian Cells. *Nano Lett.* **2006**, *6*, 662–668.
31. Rivas, L.; Sanchez-Cortes, S.; Garcia-Ramos, J. V.; Morcillo, G. Growth of Silver Colloidal Particles Obtained by Citrate Reduction to Increase the Raman Enhancement Factor. *Langmuir* **2001**, *17*, 574–577.
32. Hurst, S. J.; Lytton-Jean, A. K. R.; Mirkin, C. A. Maximizing DNA Loading on a Range of Gold Nanoparticle Sizes. *Anal. Chem.* **2006**, *78*, 8313–8318.
33. Jain, P. K.; Huang, X.; El-Sayed, I. H.; El-Sayad, M. A. Review of Some Interesting Surface Plasmon Resonance-Enhanced Properties of Noble Metal Nanoparticles and Their Applications to Biosystems. *Plasmonics* **2007**, *2*, 107–118.
34. Mie, G. Articles on the Optical Characteristics of Turbid Tubes, Especially Colloidal Metal Solutions. *Ann. Phys.* **1908**, *25*, 377–445.
35. Pillai, Z. S.; Kamat, P. V. What Factors Control the Size and Shape of Silver Nanoparticles in the Citrate Ion Reduction Method? *J. Phys. Chem. B* **2004**, *108*, 945–951.
36. Herne, T. M.; Tarlov, M. J. Characterization of DNA Probes Immobilized on Gold Surfaces. *J. Am. Chem. Soc.* **1997**, *119*, 8916–8920.
37. Cederquist, K. B.; Keating, C. D. Curvature Effects in DNA:Au Nanoparticle Conjugates. *ACS Nano* **2009**, *3*, 256–260.
38. Hill, H. D.; Millstone, J. E.; Banholzer, M. J.; Mirkin, C. A. The Role Radius of Curvature Plays in Thiolated Oligonucleotide Loading on Gold Nanoparticles. *ACS Nano* **2009**, *3*, 418–424.
39. Demers, L. M.; Mirkin, C. A.; Mucic, R. C.; Reynolds, R. A.; Letsinger, R. L.; Elghanian, R.; Viswanadham, G. A Fluorescence-Based Method for Determining the Surface Coverage and Hybridization Efficiency of Thiol-Capped Oligonucleotides Bound to Gold Thin Films and Nanoparticles. *Anal. Chem.* **2000**, *72*, 5535–5541.
40. Spitzer, S.; Eckstein, F. Inhibition of Deoxyribonucleases by Phosphorothioate Groups in Oligodeoxyribonucleotides. *Nucleic Acids Res.* **1988**, *16*, 11691–11704.
41. Radziuk, D.; Skirtach, A.; Sukhorukov, G.; Shchukin, D.; Möhwald, H. Stabilization of Silver Nanoparticles by Polyelectrolytes and Poly (ethylene glycol). *Macromol. Rapid Commun.* **2007**, *28*, 848–855.
42. Ghosn, B.; Haselton, F. R.; Gee, K. R.; Monroe, W. T. Control of DNA Hybridization with Photocleavable Adducts. *Photochem. Photobiol.* **2005**, *81*, 953–959.
43. Casey, J. P.; Blidner, R. A.; Monroe, W. T. Caged siRNAs for Spatiotemporal Control of Gene Silencing. *Mol. Pharmaceutics* **2009**, *6*, 669–685.
44. Huschka, R.; Barhoumi, A.; Liu, Q.; Roth, J. A.; Ji, L.; Halas, N. J. Gene Silencing by Gold Nanoshell-Mediated Delivery and Laser-Triggered Release of Antisense Oligonucleotide and siRNA. *ACS Nano* **2012**, *6*, 7681–7691.
45. Palankar, R.; Skirtach, A. G.; Kreft, O.; Bédard, M.; Garstka, M.; Gould, K.; Möhwald, H.; Sukhorukov, G. B.; Winterhalter, M.; Springer, S. Controlled Intracellular Release of Peptides from Microcapsules Enhances Antigen Presentation on MHC Class I Molecules. *Small* **2009**, *5*, 2168–2176.
46. Skirtach, A. G.; Antipov, A. A.; Shchukin, D. G.; Sukhorukov, G. B. Remote Activation of Capsules Containing Ag Nanoparticles and IR Dye by Laser Light. *Langmuir* **2004**, *20*, 6988–6992.
47. Skirtach, A. G.; Muñoz Javier, A.; Kreft, O.; Köhler, K.; Piera Alberola, A.; Möhwald, H.; Parak, W. J.; Sukhorukov, G. B. Laser-Induced Release of Encapsulated Materials inside Living Cells. *Angew. Chem., Int. Ed.* **2006**, *45*, 4612–4617.
48. Schwartz, J. W.; Novarino, G.; Piston, D. W.; DeFelice, L. J. Substrate Binding Stoichiometry and Kinetics of the Norepinephrine Transporter. *J. Biol. Chem.* **2005**, *280*, 19177–19184.

49. Forman, J.; Dietrich, M.; Monroe, W. T. Photobiological and Thermal Effects of Photoactivating UVA Light Doses on Cell Cultures. *Photochem. Photobiol. Sci.* **2007**, *6*, 649–658.
50. Sortino, S. Nanostructured Molecular Films and Nanoparticles with Photoactivable Functionalities. *Photochem. Photobiol. Sci.* **2008**, *7*, 911–924.
51. Myli, K. B.; Coon, S. R.; Grassian, V. H. Photon-Induced Reactions of Aromatics Adsorbed on Rough and Smooth Silver Surfaces. *J. Phys. Chem.* **1995**, *99*, 16407–16415.
52. Awazu, K.; Fujimaki, M.; Rockstuhl, C.; Tominaga, J.; Murakami, H.; Ohki, Y.; Yoshida, N.; Watanabe, T. A Plasmonic Photocatalyst Consisting of Silver Nanoparticles Embedded in Titanium Dioxide. *J. Am. Chem. Soc.* **2008**, *130*, 1676–1680.
53. Christopher, P.; Xin, H.; Linic, S. Visible-Light-Enhanced Catalytic Oxidation Reactions on Plasmonic Silver Nanostructures. *Nat. Chem.* **2011**, *3*, 467–72.
54. Thomann, I.; Pinaud, B. A.; Chen, Z.; Clemens, B. M.; Jaramillo, T. F.; Brongersma, M. L. Plasmon Enhanced Solar-to-Fuel Energy Conversion. *Nano Lett.* **2011**, *11*, 3440–3446.
55. Goncher, G. M.; Parsons, C. A.; Harris, C. B. Photochemistry on Rough Metal-Surfaces. *J. Phys. Chem.* **1984**, *88*, 4200–4209.
56. Moskovits, M. Surface-Enhanced Spectroscopy. *Rev. Mod. Phys.* **1985**, *57*, 783–826.
57. Jeong, D. H.; Suh, J. S.; Moskovits, M. Enhanced Photochemistry of 2-Aminopyridine Adsorbed on Silver Colloid Surfaces. *J. Raman Spectrosc.* **2001**, *32*, 1026–1031.
58. Watanabe, K.; Menzel, D.; Nilius, N.; Freund, H. J. Photochemistry on Metal Nanoparticles. *Chem. Rev.* **2006**, *106*, 4301–4320.
59. Crooke, S. T. *Antisense Drug Technology: Principles, Strategies, and Applications*, 2nd ed.; CRC Press Taylor & Francis Group: Boca Raton, FL, 2008.
60. Emerich, D. F.; Thanos, C. G. The Pinpoint Promise of Nanoparticle-Based Drug Delivery and Molecular Diagnosis. *Biomol. Eng.* **2006**, *23*, 171–184.
61. Wang, Y.; Wu, L.; Wang, P.; Lv, C.; Yang, Z.; Tang, X. Manipulation of Gene Expression in Zebrafish Using Caged Circular Morpholino Oligomers. *Nucleic Acids Res.* **2012**, *40*, 11155–11162.
62. Tang, X. J.; Dmochowski, I. J. Regulating Gene Expression with Light-Activated Oligonucleotides. *Mol. BioSyst.* **2007**, *3*, 100–110.
63. Blidner, R. A.; Svoboda, K. R.; Hammer, R. P.; Monroe, W. T. Photoinduced RNA Interference Using DMNPE-Caged 2′-Deoxy-2′-fluoro Substituted Nucleic Acids *In Vitro* and *In Vivo*. *Mol. BioSyst.* **2008**, *4*, 431–440.
64. Ando, H.; Furuta, T.; Tsien, R. Y.; Okamoto, H. Photomediated Gene Activation Using Caged RNA/DNA in Zebrafish Embryos. *Nat. Genet.* **2001**, *28*, 317–326.
65. Jain, P. K.; Shah, S.; Friedman, S. H. Patterning of Gene Expression Using New Photolabile Groups Applied to Light Activated RNAi. *J. Am. Chem. Soc.* **2010**, *133*, 440–446.
66. Gardner, L.; Deiters, A. Light-Controlled Synthetic Gene Circuits. *Curr. Opin. Chem. Biol.* **2012**, *16*, 292–299.
67. Parpura, V.; Haydon, P. "Uncaging" Using Optical Fibers to Deliver UV Light Directly to the Sample. *Croat. Med. J.* **1999**, *40*, 340.
68. Dong, Q.; Svoboda, K.; Tiersch, T. R.; Todd Monroe, W. Photobiological Effects of UVA and UVB Light in Zebrafish Embryos: Evidence for a Competent Photorepair System. *J. Photochem. Photobiol., B* **2007**, *88*, 137–146.
69. Alvarez-Lorenzo, C.; Bromberg, L.; Concheiro, A. Light-Sensitive Intelligent Drug Delivery Systems. *Photochem. Photobiol.* **2009**, *85*, 848–860.
70. Lee, P. C.; Meisel, D. Adsorption and Surface-Enhanced Raman of Dyes on Silver and Gold Sols. *J. Phys. Chem.* **1982**, *86*, 3391–3395.
71. Storhofff, J. J.; Elghanian, R.; Mirkin, C. A.; Letsinger, R. L. Sequence-Dependent Stability of DNA-Modified Gold Nanoparticles. *Langmuir* **2002**, *18*, 6666–6670.
72. Rusu, P. C.; Giovannetti, G.; Brocks, G. Dipole Formation at Interfaces of Alkanethiolate Self-Assembled Monolayers and Ag. *J. Phys. Chem. C* **2007**, *111*, 14448–14456.
73. Glass, J.; Wertz, G. W. Different Base per Unit Length Ratios Exist in Single-Stranded RNA and Single-Stranded-DNA. *Nucleic Acids Res.* **1980**, *8*, 5739–5751.